

**Ti-6Al-4V ALLOY COATED WITH BIOCERAMICS  
BY USING RADIOFREQUENCY PLASMA  
SPUTTERING TECHNIQUE**

by

**RAHEEM LAFTA ALI**

**Thesis submitted in fulfillment of the requirements  
for the degree of  
Doctor of Philosophy**

**December 2016**

## **ACKNOWLEDGEMENT**

Never-ending thanks and praise to Allah for providing me strength and patience to accomplish this work. Great thanks to my main supervisor, Prof. Dr. Mohamed Suhaimi Bin Jaafar, for his scholarly guidance and dedicated time and support throughout the course of this study. Thanks again prof. for having your door open every time I needed help, even though you never had the time, you always made it. My respect and appreciation are gratefully extended to Co-supervisor, Assist. Prof. Dr. Shahrom Mahmud, for his valuable guidance during the study.

My special thanks to University of Mustansiriya for a study leave to complete this Ph.D. degree and the lecturers and staff in the College of Education, Department of Physics. Far in distance and connected in hearts, My special thanks to my dear mother, brothers and sisters for their kindness, long time moral support, and unconditional love. Last, and most important, the special thanks to my wife and my children for accompanying me during this important time in our lives. Without their endless love, patience and support, I could not have a chance to complete this study.

Special thanks to all my friends and colleagues who supported me and helped me at the School of Physics in Universiti Sains Malaysia and University of Mustansiriya.

## TABLE OF CONTENTS

<b>ACKNOWLEDGEMENT</b>	ii
<b>TABLE OF CONTENTS</b>	iii
<b>LIST OF TABLES</b>	viii
<b>LIST OF FIGURES</b>	ix
<b>LIST OF ABBREVIATIONS</b>	xv
<b>LIST OF SYMBOLS</b>	Xviii
<b>ABSTRAK</b>	xix
<b>ABSTRACT</b>	xxi
<b>CHAPTER1: INTRODUCTION</b>	1
1.1 Introduction	1
1.2 Motivation and problem statements	2
1.3 Objectives of the research	3
1.4 Scope of study	4
1.5 Research originality	4
1.6 Thesis outline	5
<b>CHAPTER2: LITERATURE REVIEW AND THEORY</b>	
2.1 Introduction	7
2.2 Literature review	7
2.3 Bone	18
2.3.1 Composition	19
2.3.2 Macrostructure	19
2.3.3 Mechanical properties	20
2.3.4 Viscoelasticity of the bone	23

2.3.5 Bone Remodeling	23
2.4 Osseointegration	24
2.5 Dental Implant	24
2.5.1 Advantages of Dental Implants	25
2.6 Biocompatibility	25
2.6.1 Biocompatible Materials	26
2.7 Metals and Alloys	28
2.7.1 Titanium	30
2.7.2 Titanium alloys	33
2.7.3 Titanium dioxide surfaces	36
2.8 Corrosion resistance	36
2.9 Ceramics	37
2.9.1 Bioactive ceramics	38
2.9.2 Calcium phosphate (CaP)	39
2.9.3 Zirconia	40
2.9.4 Glass ceramics	42
2.10 Carbons	43
2.11 Composite	43
2.12 Implant surface	44
2.12.1 Types of surface modification	45
2.13 Surface treatment	46
2.13.1 Coating with TiO <sub>2</sub>	46
2.13.2 Coating with ceramic material	47
2.13.3 Hydroxyapatite coating	47
2.14 Techniques for bioceramic coatings	49

2.15 Plasma Surface Modification	50
2.15.1 Plasma Spraying	50
2.15.2 Anodic Oxidation	51
2.15.3 Plasma Nitriding	51
2.15.4 RF Plasma Deposition	52
2.15.5 Ion Implantation	52
<b>CHAPTER 3: METHODOLOGY AND INSTRUMENTATION</b>	<b>53</b>
3.1 Introduction	53
3.2 Samples preparation	53
3.2.1 Cutting	53
3.2.2 Grinding and Polishing	54
3.2.3 Etching	55
3.2.4 Cleaning	55
3.3 Synthesis of bioceramic layer on Ti-6Al-4V alloy by RF plasma method	55
3.4 Immersion test	57
3.5 Instrumentation	59
3.5.1 RF- plasma magnetron sputtering	59
3.5.2 Thickness Measurements	60
3.5.3 Structural and Morphological Characterizations	61
3.5.3(a) X-ray diffraction (XRD)	61
3.5.3(b) Atomic force microscope (AFM)	64
3.5.3(c) Field emission scanning electron microscope (FESEM) and energy dispersive X-ray (EDX) spectroscopy	65

3.6 Summary	69
<b>CHAPTER 4: RESULTS AND DISCUSSIONS</b>	<b>70</b>
4.1 Hydroxyapatite layer coated Ti-6Al-4V alloy	70
4.1.1 Introduction	70
4.1.2 X-ray diffraction analysis of bioceramic HA <sub>P</sub> coating on Ti-6Al-4V alloy	70
4.1.3 FESEM observation of bioceramic HA <sub>P</sub> coating on Ti-6Al-4V alloy	73
4.1.4 Elemental Analysis of bioceramic HA <sub>P</sub> coating on Ti-6Al-4V alloy	77
4.1.5 Thickness of bioceramic HA <sub>P</sub> coating on Ti-6Al-4V alloy	79
4.1.6 Surface roughness analysis (AFM analysis) of bioceramic HA <sub>P</sub> coating on Ti-6Al-4V alloy	80
4.1.7 Hardness characteristics of bioceramic HA <sub>P</sub> coating on Ti-6Al-4V alloy	85
4.1.8 Apatite layer formation	86
4.2 ZrO <sub>2</sub> layer coated Ti-6Al-4V alloy	91
4.2.1 Introduction	91
4.2.2 X-ray diffraction analysis of ZrO <sub>2</sub> layer coated Ti-6Al-4V alloy	91
4.2.3 FESEM observation of ZrO <sub>2</sub> layer coated Ti-6Al-4V alloy	93
4.2.4 Elemental Analysis of ZrO <sub>2</sub> layer coated Ti-6Al-4V alloy	96
4.2.5 Thickness of ZrO <sub>2</sub> layer coated Ti-6Al-4V alloy	97
4.2.6 Surface roughness analysis (AFM analysis) of ZrO <sub>2</sub> layer coated Ti-6Al-4V alloy	99
4.2.7 Hardness characteristics of ZrO <sub>2</sub> layer coated Ti-6Al-4V alloy	102

4.2.8 Apatite layer formation of ZrO <sub>2</sub> layer coated Ti-6Al-4V alloy	103
4.3 TiO <sub>2</sub> layer coated Ti-6Al-4V alloy	106
4.3.1 Introduction	106
4.3.2 X-ray diffraction analysis of bioceramic (TiO <sub>2</sub> )	106
4.3.3 FESEM observation of TiO <sub>2</sub> layer coated Ti-6Al-4V alloy	108
4.3.4 Elemental Analysis of TiO <sub>2</sub> layer coated Ti-6Al-4V alloy	111
4.3.5 Thickness of TiO <sub>2</sub> layer coated Ti-6Al-4V alloy	112
4.3.6 Surface roughness analysis (AFM analysis) of TiO <sub>2</sub> layer coated Ti-6Al-4V alloy	113
4.3.7 Hardness characteristics of TiO <sub>2</sub> layer coated Ti-6Al-4V alloy	116
4.3.8 Apatite layer formation of TiO <sub>2</sub> layer coated Ti-6Al-4V alloy	117
4.4 Comparison and discussion of physical properties of bioceramic materials (HA <sub>P</sub> , ZrO <sub>2</sub> and TiO <sub>2</sub> ) coating Ti-6Al-4V alloy	120
4.4.1 Introduction	120
4.4.2 Structures and Surface Properties Investigation	120
4.5 Summary	123
<b>CHAPTER 5: CONCLUSION AND FUTURE WORKS</b>	125
5.1 Conclusion	125
5.2 Future works	127
<b>REFERENCES</b>	128
<b>PUBLICATION</b>	145
<b>1. CONFERENCE</b>	145

## LIST OF TABLES

	<b>Page</b>
Table 2.1: Chemical Compositions of Pure Titanium.	32
Table 3.1: Composition of simulated body fluid (SBF).	58
Table 4.1: Morphological characteristics from AFM images for Ti-6Al-4V substrate and HA <sub>P</sub> coated Ti-6Al-4V alloy without and with annealing at 800 °C.	81
Table 4.2: Roughness values of Ti-6Al-4V substrate and ZrO <sub>2</sub> coated Ti-6Al-4V alloy without and with annealing at 800 °C.	99
Table 4.3: Roughness values of Ti-6Al-4V substrate and TiO <sub>2</sub> coated Ti-6Al-4V alloy without and with annealing at 800 °C.	116
Table 4.4: Comparison of surface properties of bioceramic materials (HA <sub>P</sub> , ZrO <sub>2</sub> and TiO <sub>2</sub> ) coated Ti-6Al-4V alloy without and with annealing at 800 °C.	122



## LIST OF FIGURES

	<b>Page</b>
Figure 2.1:	20
(a) The SEM image of the cortical bone from a human tibia (Andrew Syred/Photo Researchers, Inc.)	
(b) A photomicrograph of cancellous bone.	
Figure 2.2:	21
Strain curves for cortical and trabecular bones.	
Figure 2.3:	22
The stress strain curves for cortical bone samples of various orientations along the bone showing the anisotropic nature of bone L= longitudinal axis, T= aligned transverse.	
Figure 2.4:	33
An artist's view of the titanium/tissue interface. The oxide of titanium is covered with a very thin layer of titanium peroxy compounds, which are in contact with the living bone.	
Figure 2.5:	35
Titanium and its alloy for dental application.	
Figure 3.1:	54
The overall view of the dual platen grinder-polisher machine equipped with Vector power head grinder-polisher.	
Figure 3.2:	57
a) Ti-6Al-4V alloy without coating, b) Ti-6Al-4V alloy after coating with bioceramic layer of HA <sub>P</sub> , c) Ti-6Al-4V alloy after coating with bioceramic layer of ZrO <sub>2</sub> and d) Ti-6Al-4V alloy after coating with bioceramic layer of TiO <sub>2</sub> .	
Figure 3.3:	58
The immersion test in 30 ml of SBF at 37 °C and pH =7.4.	
Figure 3.4:	60
Schematic diagram of an RF magnetron sputtering system.	
Figure 3.5:	63
(a) Schematic diagram of $\theta/2\theta$ diffraction in Bragg –Brentano geometry and (b) visualization of XRD from two parallel atomic planes in crystalline material.	

Figure 3.6:	Schematic diagram of an atomic force microscope AFM.	65
Figure 3.7:	Schematic diagram of the signals generated by an FESEM when an electron beam interacts with a specimen.	68
Figure 3.8:	Schematic diagram of an EDX system.	68
Figure 4.1:	X-ray diffraction pattern of the Ti-6Al-4V alloy.	71
Figure 4.2:	X-ray diffraction pattern of HA <sub>P</sub> coated Ti-6Al-4V alloy without annealing.	72
Figure 4.3:	X-ray diffraction pattern of HA <sub>P</sub> coated Ti-6Al-4V alloy with annealing at 800 °C.	72
Figure 4.4:	FESEM images of the untreated Ti-6Al-4V substrate (a) 50k x magnification (b) 100k x magnification.	74
Figure 4.5:	FESEM images of the HAP nanostructure deposited on Ti-6Al-4V substrate without annealing (a) 50k x magnification; (b) 100k x magnification.	75
Figure 4.6:	FESEM images of the HAP nanostructure deposited on Ti-6Al-4V substrate with annealing at 800 °C (a) 100k x magnification; (b) 200k x magnification.	76
Figure 4.7:	EDX analyses of the samples of the as-received Ti-6Al-4V substrate.	77
Figure 4.8:	EDX analyses of the HA <sub>P</sub> deposited on Ti-6Al-4V substrate without annealing.	78
Figure 4.9:	EDX analyses of the HA <sub>P</sub> deposited on Ti-6Al-4V substrate with annealing at 800 °C.	78

Figure 4.10:	FESEM cross-section of the HA <sub>P</sub> nanostructure deposited on Ti-6Al-4V substrate without annealing.	79
Figure 4.11:	FESEM cross-section of the HA <sub>P</sub> nanostructure deposited on Ti-6Al-4V substrate with annealing at 800 °C.	80
Figure 4.12:	AFM images of Ti-6Al-4V substrates (a) 2D and (b) 3D.	82
Figure 4.13:	AFM images of HA <sub>P</sub> nanostructure on Ti-6Al-4V substrate without annealing with 5μm×5μm scanning area (a) 2D and (b) 3D.	83
Figure 4.14:	AFM images of HA <sub>P</sub> nanostructure on Ti-6Al-4V substrate with annealing at 800 °C with 5μm×5μm scanning area (a) 2D and (b) 3D.	84
Figure 4.15:	Results of Hardness test for Ti-6Al-4V substrate and HA <sub>P</sub> coated Ti-6Al-4V alloy without and with annealing at 800 °C.	85
Figure 4.16:	FESEM images of the Ti-6Al-4V substrate with annealing at 800 °C and immersion in SBF for 14 days (a) 50k x magnification (b) 100k x magnification.	87
Figure 4.17:	FESEM images of the HA <sub>P</sub> nanostructure deposited on Ti-6Al-4V substrate with annealing at 800 °C and immersion in SBF for 14 days (a) 50k x magnification (b) 100k x magnification.	89

Figure 4.18:	X-ray diffraction pattern of HA <sub>P</sub> coated Ti-6Al-4V alloy with annealing at 800 °C and after immersion in SBF for 14 days.	90
Figure 4.19:	EDX analyses of the HA <sub>P</sub> deposited on Ti-6Al-4V substrate after immersion in SBF for 14 days.	90
Figure 4.20:	X-ray diffraction pattern of ZrO <sub>2</sub> coated Ti-6Al-4V alloy.	92
Figure 4.21:	X-ray diffraction pattern of ZrO <sub>2</sub> coated Ti-6Al-4V alloy with annealing 800 °C.	92
Figure 4.22:	FESEM images of the ZrO <sub>2</sub> nanostructure deposited on Ti-6A-4V substrate without annealing (a) 50k x magnification; (b) 100k x magnification.	94
Figure 4.23:	FESEM images of the ZrO <sub>2</sub> nanostructure deposited on Ti-6Al-4V substrate with annealing at 800 C° (a) 100k x magnification; (b) 200k x magnification.	95
Figure 4.24:	EDX analyses of the ZrO <sub>2</sub> deposited on Ti-6Al-4V substrate without annealing.	96
Figure 4.25:	EDX analyses of the ZrO <sub>2</sub> deposited on Ti-6Al-4V substrate with annealing at 800 °C.	97
Figure 4.26:	FESEM cross- section of the ZrO <sub>2</sub> nanostructure deposited on Ti-6Al-4V substrate without annealing.	98
Figure 4.27:	FESEM cross-section of the ZrO <sub>2</sub> nanostructure deposited on Ti-6Al-4V substrate with annealing at 800 °C.	98
Figure 4.28:	AFM images of ZrO <sub>2</sub> nanostructure on Ti-6Al-4V substrate without annealing with 5µm×5µm scanning area (a) 2D and (b) 3D.	100

Figure 4.29:	AFM images of ZrO <sub>2</sub> nanostructure on Ti-6Al-4V substrate with annealing at 800 °C with 5µm×5µm scanning area (a) 2D and (b) 3D.	101
Figure 4.30:	Results of Hardness test for Ti-6Al-4V substrate and ZrO <sub>2</sub> coated Ti-6Al-4V alloy without and with annealing at 800 °C.	102
Figure 4.31:	FESEM images of the ZrO <sub>2</sub> nanostructure deposited on Ti-6Al-4V substrate showing surface after immersion in SBF for 14 days (a) 50k x magnification; (b) 100k x magnification.	104
Figure 4.32:	EDX analyses of the ZrO <sub>2</sub> deposited on Ti-6Al-4V substrate with annealing 800 °C after immersion in SBF for 14 days.	105
Figure 4.33:	X-ray diffraction pattern of ZrO <sub>2</sub> coated Ti-6Al-4V alloy with annealing 800 °C after immersion in SBF for 14 days.	105
Figure 4.34:	X-ray diffraction pattern of TiO <sub>2</sub> coated Ti-6Al-4V alloy	107
Figure 4.35:	X-ray diffraction pattern of TiO <sub>2</sub> coated Ti-6Al-4V alloy with annealing 800°C.	107
Figure 4.36:	FESEM images of the TiO <sub>2</sub> nanostructure deposited on Ti-6Al-4V substrate without annealing (a) 100k x magnification; (b) 200k x magnification.	109
Figure 4.37:	FESEM images of the TiO <sub>2</sub> nanostructure deposited on Ti-6Al-4V substrate with annealing 800 °C (a) 100k x magnification; (b) 200k x magnification.	110
Figure 4.38:	EDX analyses of the TiO <sub>2</sub> deposited on Ti-6Al-4V substrate without annealing.	111

Figure 4.39:	EDX analyses of the TiO <sub>2</sub> deposited on Ti-6Al-4V substrate with annealing at 800 °C.	112
Figure 4.40:	FESEM cross- section of the TiO <sub>2</sub> nanostructure deposited on Ti-6Al-4V substrate without annealing (100k x magnification).	112
Figure 4.41:	FESEM cross- section of the TiO <sub>2</sub> nanostructure deposited on Ti-6Al-4V substrate with annealing at 800 °C.	113
Figure 4.42:	AFM images of TiO <sub>2</sub> nanostructure on Ti-6Al-4V substrate without annealing with 5µm×5µm scanning area (a) 2D and (b) 3D.	114
Figure 4.43	AFM images of TiO <sub>2</sub> nanostructure on Ti-6Al-4V substrate with annealing at 800 °C with 5µm×5µm scanning area (a) 2D and (b) 3D.	115
Figure 4.44	Results of Hardness test for Ti-6Al-4V substrate and TiO <sub>2</sub> coated Ti-6Al-4V alloy without and with annealing at 800 °C.	117
Figure 4.45	FESEM images of the TiO <sub>2</sub> nanostructure deposited on Ti-6Al-4 alloy showing surface after immersion in SBF for 14 days (a) 50k x magnification;.(b).100k x magnification.	118
Figure 4.46	EDX analyses of the TiO <sub>2</sub> deposited on Ti-6Al-4V substrate and annealing at 800 °C after immersion in SBF for 14 days.	119
Figure 4.47	X-ray diffraction pattern of TiO <sub>2</sub> coated Ti-6Al-4V alloy and annealing at 800 °C after immersion in SBF for 14 days.	119

## LIST OF ABBREVIATIONS

AFM	Atomic force microscope
a.u.	Arbitrary unit
Ar	Argon
AS	Aperture slit
ASTM	American society for testing and material
Bcc	Body-centered cubic
Bses	Backscattered electrons
C	Cubic
CpTi	Commercially pure titanium
CVD	Chemical vapor deposition
ECR	Electron cyclotron resonance
EDX	Energy dispersive x-ray
EIS	Electrochemical impedance spectroscopy
EPD	Electrophoretic deposition technique
FESEM	Field emission scan electron microscope
FT-IR	Fourier transform infrared spectroscopy
HA <sub>p</sub>	Hydroxyapatite
Hcp	Hexagonal close-packed
HV	Vickers pyramid number
IBAD	Ion beam assisted deposition
Iols	Intraocular lenses
ISO	The international organization for standardization

JCDD	Joint committee on powder diffraction standards
JCPDS-ICDD	International Centre for Diffraction Data
L	Longitudinal axis
M	Monoclinic
MPa	Megapascal
P	Pressure
PBS	Phosphate buffered saline
PEO	Plasma electrolytic oxidation
PIII&D	Plasma immersion ion implantation and deposition
PIRAC	Powder immersion reaction assisted coating
PLD	Pulsed laser deposition
PSII	Plasma source ion implantation
Psz	Partially stabilized zirconia
PVD	Plasma vapor deposition
Rf plasma	Radio frequency plasma
rfGD	Radio frequency glow discharge
RMS	Root mean square
rpm	Rotations per minute
SBF	Simulated body fluid
Sccm	Standard cubic centimeters per minute
SEM	Scanning electron microscope
Ses	Secondary electrons
Sic	Silicon carbide
T	Tetragonal
TCP	Tricalcium phosphate



Tjrs	Total joint replacements
USM	Universiti Sains Malaysia
W	Watt
XRD	X ray diffraction

## LIST OF SYMBOLS

$\beta$	Full-width at half-maximum
$\theta$	Bragg's angle
$\lambda$	Wavelength
$\lambda D$	Debye length
$^{\circ}\text{C}$	Celsius temperature
$a, c$	Lattice constants
Cjs111a	Ball-disk wear instrument
$h, k, l$	Miller's indices
$k$	Boltzman constant
Ti-6Al-4V	Titanium-aluminum-vanadium alloy
TNTs	TiO <sub>2</sub> nanotubes

# **ALOI Ti-6Al-4V TERSALUT DENGAN BIOSERAMIK MENGGUNAKAN TEKNIK PERCIKAN PLASMA RADIOFREKUENSI**

## **ABSTRAK**

Biobahan adalah bahan sintetik yang digunakan untuk menggantikan sebahagian organ hidup atau berfungsi secara intim dengan tisu hidup. Aloi titanium dan Ti-6Al-4V adalah di antara bahan implan yang paling kerap digunakan, disebabkan oleh rintangan kakisan yang baik, kekuatan dan kekenyalan yang sangat baik. Elemen-elemen aloi Ti-6Al-4V membawa kepada respon alergik dan degenerasi tisu otot. Pembebasan elemen-elemen ini ke dalam sistem tubuh badan boleh membawa maut untuk aplikasi jangka-panjang aloi ini ke dalam tubuh manusia. Maka itu, tujuan kajian ini ialah untuk memperbaiki ciri-ciri struktur dan bio-kesesuaian bioseramik yang disadur dengan Ti-6Al-4V dengan menggunakan teknik RF plasma frekuensi radio. Penyepuhlindapan filem-filem yang berdesir adalah penting untuk mengubah saduran amorfus kepada saduran kristalin. Selepas pencekalan, morfologi, ketebalan, kekasaran permukaan dan analisis struktur filem-filem ini dicirikan menggunakan Field Emission Scanning Electron Microscopy (FESEM), Atomic Force Microscope (AFM) dan belauan sinar-X (XRD), masing-masing. Pada penyepuhlindapan 800, FESEM, AFM dan XRD menunjukkan bebas retak dan pori dalam lapisan nipis HA<sub>p</sub>, bersadur dengan aloi Ti-6Al-4V dan indeks-indeks Miller (hkl): (002), (211), (301) dan (004), masing-masing. Ia menjadi milik fasa HA<sub>p</sub> yang membuktikan bahawa data yang dilaporkan untuk (JCDs-ICDD file # 09-0432) berbentuk heksagon. Fasa TiO<sub>2</sub> adalah fasa dominan pola XRD TiO<sub>2</sub> bersadur aloi Ti-6Al-4V pada penyepuhlindapan 800. Lapisan nipis (HA<sub>p</sub>, ZrO<sub>2</sub> dan TiO<sub>2</sub>) meningkat dengan peningkatan pada penyepuhlindapan 800. Kekerasan spesimen yang dirawat dan tidak dirawat telah ditentukan oleh kekerasan Vicker.

Selepas penyepuhlindapan, nilai kekerasan bahan bioseramik bi ( $\text{HA}_p$ ,  $\text{ZrO}_2$  dan  $\text{TiO}_2$ ) bersadur aloi Ti-6Al-4V ialah 780, 560 dan 470 Hv, masing-masing. Lapisan-lapisan ini didapati lebih keras daripada substrat Ti-6Al-4V (348.9 Hv). Selepas penyepuhlindapan pada 800, nilai kekasaran bahan bioseramik ( $\text{HA}_p$ ,  $\text{ZrO}_2$  dan  $\text{TiO}_2$ ) bersadur aloi Ti-6Al-4V adalah 245nm, 166.8 dan 38.4, masing-masing. Biokesesuaian sampel ditentukan oleh ujian rendaman sampel dalam bendalir tubuh yang disimulasi pada suhu dan pH yang hampir dengan tubuh manusia. Bioseramik yang disadur dengan aloi, yang bebas dari rekahan dan pori, bertindak sebagai motivasi fizikal untuk mencipta lapisan apatit ke atas permukaan aloi. Keputusannya mungkin penting untuk memperbaiki ciri-ciri bio-kesesuaian jangka panjang bahan dan untuk meningkatkan lagi lapisan apatit ke atas permukaan yang dirawat. Keputusan kajian ini menyumbang kepada ilmu baru ke atas modifikasi permukaan bioseramik yang bersadur dengan aloi titanium.

# **Ti-6Al-4V ALLOY COATED WITH BIO-CERAMIC BY USING RADIOFREQUENCY PLASMA SPUTTERING TECHNIQUE**

## **ABSTRACT**

Biomaterials are synthetic materials used to replace part of a living organ or to function in intimate contact with living tissue. Titanium and Ti-6Al-4V alloy are among the most commonly used implant materials, because of the good corrosion resistance, excellent strength and ductility. Elements of Ti-6Al-4V alloy cause allergic response and degeneration of muscle tissue. The subsequent release of these elements into the body system is fatal for the long term application of this alloy in the human body. Therefore, the aim of this study was to improve the structure properties and the biocompatibility of bioceramic coated Ti-6Al-4V by using radio frequency plasma technique RF. Annealing of the as-sputtered films was necessary to change the amorphous coating to a crystalline coating. After annealing, the morphology, the thickness, the roughness surface and structure analysis of these films were characterized using the Field Emission Scanning Electron Microscopy (FESEM), Atomic Force Microscope (AFM) and X-ray diffraction (XRD), respectively. At annealing 800°C, FESEM, AFM and XRD showed free of cracks and pores in the HA<sub>p</sub>, thin film coated Ti-6Al-4V alloy and the following Miller indices (hkl): (002), (211), (301) and (004), respectively. They belong to the HA<sub>p</sub> phase which proved the data reported for hexagonal Ca<sub>5</sub>(PO<sub>4</sub>)<sub>3</sub>OH (JCDS-ICDD file # 09-0432). TiO<sub>2</sub> phase was the dominant phase in all XRD patterns of TiO<sub>2</sub> coated Ti-6Al-4V alloy at annealing 800°C. The hardness of the untreated and treated specimens was determined by Vicker's hardness. After annealing, the hardness values of the bioceramics materials (HA<sub>p</sub>, ZrO<sub>2</sub> and TiO<sub>2</sub>) coated Ti-6Al-4V alloy

were 780, 560 and 470 Hv, respectively. These layers were found to be more hardness than the Ti-6Al-4V (348.9 Hv) substrate. After annealing at 800°C, the roughness values of bioceramic materials (HA<sub>p</sub>, ZrO<sub>2</sub> and TiO<sub>2</sub>) coated Ti-6Al-4V alloy were 245, 166.8 and 38.4 nm, respectively. The biocompatibility of the samples was determined by immersion test of the samples in simulated body fluids at temperature and pH close to the human body. The bioceramic coated alloy, which is free of cracks and pores, acts as physical motivation to create apatite layer on the alloy surface. The results might be of great importance to improve the long-term biocompatibility properties of the material and to enhance the apatite layer on the treated surface. The results of this research contribute new knowledge on the surface modification of bioceramic coated titanium alloy.

## CHAPTER 1

### INTRODUCTION

#### 1.1 Introduction

The biomaterials are of immense importance for the mankind in general but specifically for the existence and longevity of some of the less fortunate human beings, who even at the time of birth are born with congenital heart disease and also for the aged population who require biomedical implants to increase their life span. The people need the help of geriatric physicians for several ailments as the parts of the human body organs have performed their expected tasks for long years and have become worn out. Especially after the wars, the need for biomaterials was acutely felt this field assumes much more significance (Manivasagam et al., 2010)

Bioimplant is commonly used in dentistry, orthopedics, plastic and reconstructive surgery, ophthalmology, cardiovascular surgery, neurosurgery, experimental surgery, and veterinary medicine. Many types of materials, such as metals and ceramics are used as biomaterials. Metals are used in weight bearing applications, i.e. as bone implants. The perfect bone implant material has not yet been developed. All the biomaterials used in bone tissue tend to loosen over time. The interactions of implant materials and tissues are complex and they vary depending on both the implant material and target tissue (Adamus, 2007). Metals (biomaterials) are the most suitable for replacing failed hard tissue up to now.

Dental implants are currently the most innovative and exciting treatment modality in dentistry. They are being widely used for a variety of indications, and most of the various techniques in use are evidence based and

predictable (Stanford, 2010). Titanium and its alloys are widely used as dental implant materials because of their suitable mechanical properties and good biocompatibility. The latter is mainly due to reduce the release metallic ions in the physiological environment by a tenacious layer of titanium dioxides that appear on the implant's surface immediately after exposure to oxygen (Athraa et al., 2011).

## **1.2 Motivation and problem statements**

Ti-6Al-4V alloy has been increasingly used in the medical devices industry. The effect of good biocompatibility of Ti-6Al-4V alloy was the driving forces for its early application in medical implants. Ti-6Al-4V alloy exhibits excellent corrosion resistance, wear resistance and mechanical properties. Many successful medical applications of Ti-6Al-4V alloy have been investigated recently. The Ti-6Al-4V alloy can be applied for the manufacturing of equipment and devices used for medical applications in dentistry (Shahram, 2010).

Ti-6AL-4V alloy exhibits desirable and superior properties for medical application, however, the existence of high concentration of titanium, aluminum and vanadium in the Ti-6Al-4V alloy has hindered its use for long term implantation (Xuanyong, 2004). It has been reported that the amount of elements content in the alloy may be released in vivo environment and this releasing of alloy elements may induce toxic and allergic response to body tissues. The subsequent release of ions into the body system is an important issue for long term application of this alloy in the human body.

There is a current challenge to develop biomaterials for long-term implantation. However, the surface of the Ti-6Al-4V can be covered with another



biomaterial to improve the surface properties without changing the bulk composition of the alloy, it will be most advantageous. The created apatite layers are believed to have an ability to provide a favorable environment for osteoblasts and they prevent the ions released inside the body (Xuanyong et al., 2010).

For many different types of surface treatment, RF plasma has been shown to be a viable mean for transforming the surface properties of materials. The RF plasma modification (RF plasma) is an effective and economical surface treatment technique for many materials and of growing interests in biomedical engineering. RF plasma is often used to form ceramic coatings and is the most popular technology commercially used for depositing bioceramic (hydroxyapatite HA<sub>p</sub>, zirconium ZrO<sub>2</sub> and titanium dioxide TiO<sub>2</sub>) coatings onto titanium-base and other metal-base implants. The bulk properties of Ti-6Al-4V alloy will not be affected after coating treatment. RF is able to enhance the surface properties of Ti-6Al-4V alloy without disturbing the bulk properties (Sun, 2010).

### **1.3 Objectives of the Research**

The present study was carried out to modify the surface of Ti-6Al-4V alloy to enhance physical properties by using RF plasma process with a RF power 200 W for 1h duration room temperature RT. A base pressure was evacuated to ( $1 \times 10^{-5}$  mbar). Argon gas (Ar) was passed till the pressure reached ( $1 \times 10^{-3}$  mbar) and it was supplied as reactive gas at a flow ratio of 10 sccm.

The study focused on bioceramic layer (HA<sub>p</sub>, ZrO<sub>2</sub> and TiO<sub>2</sub>) coated titanium alloy in terms of thickness, defects, structure, crystal structure, topography and composition profile.

The objectives of the present study include:

- a. To study the surface properties of bioceramic layer (HA<sub>p</sub>, ZrO<sub>2</sub> and TiO<sub>2</sub>) coated Ti-6Al-4V alloy before and after annealing at 800 °C.
- b. To evaluate the bioceramic layer coated Ti-6Al-4V alloy and to compare with untreated specimen using immersion method in simulated body fluid (SBF).

#### **1.4 Scope of study**

This study focused on the synthesis of bioceramic layer (HA<sub>p</sub>, ZrO<sub>2</sub> and ZrO<sub>2</sub>) coated titanium alloy (Ti-6Al-4V) by radio frequency plasma at growth conditions (RF power 200 W, argon pressure ( $1 \times 10^{-3}$  mbar) and flow ratio of 10 sccm). Study the surface properties of of bioceramic layer (HA<sub>p</sub>, ZrO<sub>2</sub> and ZrO<sub>2</sub>) coated titanium alloy (Ti-6Al-4V) after annealing at 800 °C. The parameters were optimized to control the crystal structure, surface morphology and biocompatibility of bioceramic layer coated Ti-6Al-4V alloy. The optimal properties were then selected to create apatite layer on the treated surface.

#### **1.5 Research originality**

The originality of this research is based on the following points:

- a. Growth of high quality and nanostructure of bioceramic layer coated Ti-6Al-4V alloy.
- b. Study of the influence of heat treatment on the crystal structure, surface morphology and biocompatibility of bioceramic layer coated Ti-6Al-4V alloy and determined the specified value of temperature, which, has not been reported before to obtain bioceramic materials with high crystallinity.

- c. Study of the effects of simulated body fluid on untreated and treated alloy by using immersion test.

## **1.6 Thesis outline**

Chapter 1 includes a brief overview of the biomaterials and their applications. Research motivation, research problem and the objectives of the study are also discussed in this chapter. Chapter 2 focuses on the literature review of some properties of biomaterials prepared by different techniques. The study of bioceramic coated titanium alloy is also included. It discusses the growth mechanism of bioceramic on material alloys by different techniques. The theoretical background of crystalline bioceramic and its application in medical science and in particular, dental science were explained. Chapter 3 describes the synthesis of bioceramic layer on Ti-6Al-4V alloy by RF plasma sputtering technique at different deposition temperatures. Also, the description on the fabrication of apatite formation on the surface of immersed samples in a simulated body fluid (SBF).

Chapter 4 provides information on the effect of hydroxyapatite layer on the surface of Ti-6Al-4V alloy on the structural properties, morphological and biocompatibility before and after annealing. Chapter 5 presents the effects of zirconium dioxide ( $ZrO_2$ ) layer coated Ti-6Al-4V alloy by RF plasma sputtering on the structural and biocompatibility properties at room temperature RT of substrate and also it discusses the effect of annealing temperature on the crystal structure before and after immersion in SBF. Chapter 6 is devoted to the effect of  $TiO_2$  layer coated Ti-6Al-4V alloy by RF plasma sputtering on the structural and biocompatibility properties.

Chapter 7 discusses the comparison of bioceramic materials (HAp, ZrO<sub>2</sub> and TiO<sub>2</sub>) layer grown on Ti-6AL-4V substrate by using RF plasma method at RT. It examines the effect of annealing temperature at 800 °C on the crystal structure, surface morphology and biocompatibility properties. The effects of bioceramic layer on the above properties are also investigated in this chapter after immersing samples in SBF. Chapter 8 presents the conclusions and suggestions for further researches in this area.

## CHAPTER 2

### LITERATURE REVIEW AND THEORY

#### 2.1 Introduction

The biomaterials are the materials that interact with human tissue and body fluids to treat, improve, or replace anatomical element(s) of the human body. Biomaterial devices used in dentistry and orthopedics are called implants. Clinical results in orthopedics have demonstrated that a great need exists to find new and better biomaterials that will help satisfy the minimum requirements for orthopedic devices to perform correctly on a long-term basis (Bajpai et al. 2010). This chapter presents a summary and review of articles concerning the preparation and synthesis of biomaterials and theoretical background.

#### 2.2 Literature review

Vardiman et al., (1981) investigated the effect of nitrogen and carbon ion implantation on the fatigue life of Ti-6Al-4V alloy. Their study suggests that ion implantation with both nitrogen and carbon increased the fatigue life of this alloy. It has been shown that nitrogen ion implantation can significantly improve the corrosive wear performance of surgical Ti-6Al-4V alloy producing a decrease by a factor of 500 in the wear rate. This improved wear resistance is accomplished by means of low friction oxide layer, which forms in the wear track.

Kenneth et al., (1991) studied on the two most widely used titanium alloys, Grade 2 commercially pure titanium CpTi and the age-hard enable Ti-6Al-4V. Dry sand-rubber wheel tests were conducted to assess abrasion resistance; fretting and

galling. Reciprocating pin-on-plane tests were conducted to determine if there is the better counterface for these two titanium alloys. The test results are distilled into recommendations for use of titanium alloys in tribosystems in the chemical process industry. The result of this study showed that both alloys have poor abrasion resistance. Grade 2 pure titanium should be avoided in all titanium tribosystems and there are preferred counterfaces for the Ti-6Al-4V alloy, but the best metal-to-metal wear resistance is obtained when the alloy is anodized and coated with a dry film lubricant.

Yoshimitsu et al., (1993) studied the effects of alloying elements other than Al and V on microstructure. Mechanical properties were investigated to develop alternative titanium alloys with higher biological safety, strength and ductility for medical implants. The strength at room temperature increases with increasing Zr content, the changes of volume fraction of  $\beta$  phase suggested that the refinement of  $\beta$  phase contributes to the increase of strength at room temperature.

Bekir et al., (1996) investigated the tribological and mechanical properties of plasma-nitride Ti-6Al-4V alloy. Samples were nitrided in an  $H_2-N_2$  (1:8 ratio) plasma. The gas of nitrogen concentration along the nitride zone was obtained using the nuclear reaction analysis technique. The temperature was varied from 450 to 520 °C during the nitriding process. Pin-on-disc wear tests were carried out to evaluate the wear properties of the resultant specimens and a ball-on-disc experiment was conducted to measure the friction coefficient. Microhardness test, Scanning electron microscope and X-ray diffraction were carried out to show the phases developed in the nitride zone.

It was found that the wear resistance improved considerably after the nitriding processes. Three distinct layers were identified:

- a. an inner layer where  $\delta$ -TiN +  $\epsilon$ -Ti<sub>2</sub>N phases formed,
- b. an intermediate layer where  $\alpha$ -(TiN) with or without  $\epsilon$  phase developed
- c. an outer layer where precipitations were dominant.

Leitao et al., (1995) studied the effect of nitrogen ion implantation on the electrochemical behavior of Ti-6Al-4V and Ti-5Al-25Fe surgical alloys in a simulated physiological solution (HBSS-Hank's balanced salt solution). They recommended that implantation of  $10^{16}$  ions/cm<sup>2</sup> N<sup>+</sup> improve the corrosion resistance of both alloys surface. The resistance of more stable oxide film formed during the ion implantation explained this kind of behavior.

Shenhar et al., (2000) studied Titanium and Ti-6Al-4V alloy samples that were coated by using a Powder Immersion Reaction Assisted Coating (PIRAC) nitriding method in order to modify their surface properties. Depending on the processing temperature, strongly adherent single (TiN) - or double (Ti, N/TiN)-layer coatings were obtained on both substrates. The result of the research suggests that titanium nitride PIRAC coatings can provide surgical titanium alloys with the longed-for fretting wear and corrosion resistant surface thereby minimizing the ion- and particulate-generating potential of modular orthopedic implants.

Thair et al., (2002) studied the effect of nitrogen ion implantation on the corrosion behavior of the as-cast Ti-6Al-7Nb alloy. Their study shows that the surface modification of Ti-6Al-7Nb alloy with nitrogen ions is considered as a method to improve its performance with respect to corrosion. The implanted

specimens were subjected to electrochemical study in Ringers solution in order to determine the optimum nitrogen ion dose that can give good corrosion resistance in a simulated body fluid condition in comparison with un-implanted specimens.

Nelut et al., (2002) studied the electrochemical behavior of Ti and Ti-7Al-4.5V and Ti-5Al-2.5Fe alloys in biological media using electrochemical impedance spectroscopy (EIS). The impedance data were fitted using an equivalent circuit, which takes into account the contribution of the space charge layer. The influence of the alloying elements is reflected in increasing resistance of the oxide film and in the growth rate.

Tan et al., (2003) demonstrated the combined influence of PSII surface modification and heat treatment on pitting corrosion and wear-corrosion resistance in NiTi through potentiodynamic polarization testing, wear-corrosion testing and surface analysis techniques. Oxygen-implanted samples with  $A_f = 21$  °C and  $1 \times 10^{17}$  ions/cm<sup>-2</sup> dose showed the higher pitting corrosion resistance, the better wear corrosion resistance in this work.

Borgioli et al., (2004) compared the effects of glow-discharge and furnace processes, performed using air as treatment atmosphere, on the microstructure and mechanical properties of Ti-6Al-4V alloy samples. Samples show comparable hardness profiles when the furnace process is performed for 4 hours and the plasma treatment was carried out for 2 hours.

Seung et al., (2005) showed that the treatment of TiO<sub>2</sub> with NaOH solution induce growth of HAp (bone-like calcium phosphate) in a SBF.



Poudel et al., (2005) indicated that the rutile phase begin to crystallize at 800 °C, a change from nanotubes to nanowire morphology was observed at the annealed temperature of 650 °C. Further comparisons in this research also present that TNTs are less stable under oxygen than under vacuum.

Prabakaran et al., (2006) developed HA<sub>p</sub> powder from fishbone through heat treatment method. Presences of characteristic peaks for hydroxyl and phosphate groups were identified by FT-IR studies. XRD analysis reveals the formation phase pure HA<sub>p</sub> at 900°C. Electrochemical study results have indicated the efficiency of fishbone-originated HA<sub>p</sub> coatings on 316L stainless steel surface.

Trtica et al., (2006) studied the effects of Nd:YAG laser interaction with titanium target using laser radiation at wavelengths of 1.064 or 0.532 μm (40 ps pulse duration). Modification of target surfaces at laser energy densities of 2.4 and 10.3 J/cm<sup>2</sup> ( $\lambda_1^{\text{laser}} = 1.064 \mu\text{m}$ ) and 1.1 J/cm<sup>2</sup> ( $\lambda_2^{\text{laser}} = 0.532 \mu\text{m}$ ) were reported in this article. Qualitatively, the Ti surface modification can be summarized as follows:

- a. Ablation of the Ti surface in the central zone of the irradiated area for laser wavelengths
- b. Appearance of a hydrodynamic feature like resolidified droplets of the material ( $\lambda_1^{\text{laser}} = 1.064 \mu\text{m}$ ), as well as formation of the wave-like microstructures ( $\lambda_2^{\text{laser}} = 0.532 \mu\text{m}$ )
- c. Appearance of plasma, in front of the Ti target, with both laser wavelengths.

Seunghan et al., (2006) demonstrated that the adhesion/propagation of the osteoblast cells is significantly improved by the topography of the nanotubes with the filopodia of the growing cells. Actually, it goes into the nanotube pores, producing an interlocked cell structure. The number of the adhered cells on the TiO<sub>2</sub> nanotubes increases significantly by 300–400% as compared to the cells adhering to the Ti metal surface, which is most likely caused by the pronounced topological feature.

Abualnoun et al., (2007) investigated the influence of heat treatment conditions on microstructure of Ti-6Al-7Nb Alloy, as used the surgical implant materials. The most common microstructure relevant to Ti-6Al-7Nb alloy are the transformed beta and equated (alpha-beta) region which have been widely used as an effective strengthening method for alpha-beta alloys.

Koyuncu (2008) studied the surface hardening of Ti-6Al-4V titanium alloy by plasma nitriding technique. The results of the examinations of microstructures, micro-hardness, thicknesses, X-Ray diffraction analyses, wear behaviors of surface layers formed on the Ti-6Al-4V titanium alloy by plasma nitriding. By using the optical micrograph two layers were determined on the samples that called compound and diffusion layers. Compound layer contain Titanium nitrides, X-ray diffraction (XRD) results support in this formations. XRD analysis showed that increasing the nitriding temperature resulted in the increase of the growth of these phases. By micro-hardness measurements investigations, the surface hardness was found to increase with increasing process temperature and time. Also the case depth was found to increase with increasing process temperature and time. The result of wear tests which was carried out using ball-on-disc machine is wear resistance of Ti-6Al-4V alloy increases as the time and temperature of plasma nitride increase.

Ogawa et al., (2008) have prepared Ti nanostructure by physical vapor deposition and tested their osseointegration in femur of rats. They found an increased surface area by up to 40 % and a greater strength of osseointegration for the nanostructured compared to an acid-etched surface.

Wang et al., (2008) showed that HA<sub>p</sub> coating can be deposited on anodized titanium by electro deposition in an electrolyte containing calcium and phosphate ions. The surface morphology of TiO<sub>2</sub> nanotube promotes mechanical interlocking between HA<sub>p</sub> and TiO<sub>2</sub>. The deposited crystals are anchored in and between the tubes. The insert mode makes a contribution to the improvement of bonding strength.

Abdul-Hameed et al., (2008) evaluated the effect of biomimetic calcium phosphate coating on the bone-implant interface of screw-shaped implants made from CpTi and Ti-6Al-7Nb alloy by histological analysis with optical microscope. The screws were biomimetically coated with calcium phosphate by immersion in a concentrated SBF (5 times), which simulates the component of human blood plasma, under static conditions in a biological thermostat at 37 °C for 6 days. The uncoated screws were passivated with 28% nitric acid. The tibias of 15 white New Zealand rabbits were chosen as implantation sites, the results obtained from this experiment revealed that the coated Ti-6Al-7Nb alloy implants had better properties than the coated CpTi implants.

Ioan-Viorel et al., (2009) evaluated the influence of Al, V, Nb and Ni alloying elements on electrochemical behavior and surface properties for Ti-Al-V, Ti-Al-Nb and Ti-Ni Natinol-like alloys. These alloys are used in orthopedic surgery for total hip and knee replacement. The utilization of Al and Nb, as alloying elements, leads to the obtaining of an alloy, Ti-Al-Nb, similar to the classic one, Ti-

Al-V, but more secure from toxicity point of view, knowing that Nb is less toxic than V. From the corrosion resistance, biocompatibility and surface properties point of view, Ti-Al-Nb alloy can be considered the most secure representative of Ti based alloys class used in orthopedic surgery.

Li-juan et al., (2009) investigated the microstructure and properties of a series of binary Ti-Nb alloys for dental prostheses with niobium contents ranging from 5% to 20%. The increase of Nb content modifies the microstructure of Ti-Nb alloys significantly and decreases their compression elastic modulus, in which Ti-20Nb alloy shows the largest compression strength and Ti-5Nb alloy shows the best plasticity. The dry sliding wear tests of these alloys against Gr15 ball were investigated on ball-disk wear instrument. For Ti-Nb alloys, Ti-10Nb alloy shows the smallest steady friction coefficient, Ti-5Nb alloy shows the smallest wear depth and the best wear resistance, and Ti-15Nb alloy shows the largest wear depth and the worst wear resistance. The furrow cut phenomenon happens and furrows form during wear test.

Kodama et al., (2009) have suggested that TiO<sub>2</sub> layer can significantly stimulate formation of apatite layers by soaking in SBF comparing with oxide layer on titanium.

Kubo et al., (2009) observed a substantial increase by 3.1 times in bone-titanium interfacial strength by TNTs (300 nm) at 2 weeks of implantation in femur rats. This result suggests the establishment of nanostructured surfaces for improved osteoconductivity. It has been also shown that various nano morphological features of titania nanotubes, such as length, diameter, wall thickness, have a major impact on

the cellular responses, providing the evidence that cells are susceptible to nanoscale dimensions (Brammer et al., 2009).

Xiao et al., (2009) invented a new method to incorporate HA<sub>p</sub> inside TNTs. Embedded-style HA<sub>p</sub>-titania nanotube arrays composite material was prepared by centrifugal filling HA<sub>p</sub> precursor sol into the nanotubes of titania nanotube arrays, with the aid of the pressure provided by a centrifuge.

Guo et al., (2009) evaluated and compared the effects of biomimetically and electrochemically deposited nano-HA<sub>p</sub> coatings on the osseointegration of porous titanium implants after 6 and 12 weeks of insertion in a rabbit bone model. Histological observation showed bone growth along the surfaces after 6 weeks. New bones were also seen on the biomimetically deposited CaP and electrochemically deposited HA<sub>p</sub> implant surfaces in the marrow space. New bone on the roughened and electrochemically deposited HA<sub>p</sub> implants became mature after 12 weeks. These results suggest that the electrochemically deposited HA<sub>p</sub> coating has a better bone integration potential than does the biomimetically deposited CaP coating.

Gabriela et al., (2010) has investigated the niobium (Nb) additions effect on both microstructure and heat-treated Ti-10Mo-xNb (x = 3, 6 and 9) alloys mechanical properties. The microstructures were characterized by optical microscope, X-ray diffraction and transmission electron microscope. The mechanical characterization was carried out by Vickers micro-hardness test and Young's modulus measurements. The results show that the addition of Nb in alloys decreased the proportion of  $\omega$  and  $\alpha'$  phases. The Ti-10Mo-3Nb alloy showed the best hardness and elastic modulus combination among the three developed alloys and also with respect to commercially pure Ti.

Figueiredo et al., (2010) showed that the calcination temperature highly conditions the properties of the bone which derived from (human and animal). As expected, higher temperatures lead to more pure forms of HAp, with higher crystallinity degrees and larger crystallite sizes and a less porous structure. Furthermore, samples heated to the same temperature exhibit similar characteristics, regardless their origin. FT-IR spectra indicate that the organic constituents are no longer present in the samples calcined at 600 °C, suggesting that this temperature is adequate to obtain protein-free samples. Moreover, these spectra have also revealed that, at this temperature, a carbonate apatite is obtained, being the carbonate removed from the mineral at higher temperatures. Furthermore, no new mineral phases were evident at higher temperatures, in good agreement with the results of thermal analysis and XRD.

Raghunandan et al., (2011) studied in vitro electrochemical behavior of a new titanium based  $\alpha$ -alloy (Ti-0.5 wt% Si-0.65 wt% C), fabricated via casting and rapid cooling route, determined using linear, Tafel, potentiodynamic polarization tests and electrochemical impedance spectroscopy (EIS), complemented with ex situ SEM-EDS analysis to evaluate the corrosion mechanism. The experimental results revealed that silicon, carbon and titanium, resulted in the enhancement of mechanical properties. The polarization tests confirmed that Ti-Si-C alloy possessed excellent corrosion resistance (a low corrosion current density of  $0.033 \mu \text{ A cm}^{-2}$ ), comparable to CpTi and it is better than Ti-6Al-4V in phosphate buffered saline (PBS). The present work reveals that Ti-Si-C alloy has a good potential for orthopedic applications, based on its mechanical properties, in vitro corrosion and mineralization behavior. Further, the biomedical potential should be manifested by in

vitro experiments with osteoblast/fibroblast cells as a next step towards the application in human medicine.

Juraida et al., (2011) showed that fishbone can be used as a natural source for production of HA<sub>p</sub>. HA<sub>p</sub> from fishbone was prepared and characterized using four different instruments. Three different sized 25μm, 90μm and 150μm were prepared and the best sized that produced a good quality of HA<sub>p</sub> was chosen and compared with four different temperatures which are 800 °C, 900 °C, 1000 °C and 1100 °C. Based on the FT-IR analysis, 25μm has the lowest intensity compared to the other two sizes and the highest temperature of 1100 °C has the lowest intensity and lowest impurity is the good quality of HA<sub>p</sub>.

Yaarob et al., (2011) used EPD to obtain a uniform coating of HA<sub>p</sub> on the tapered Ti-6Al-7Nb screws. In vivo the study was performed by the implantation of tapered screw-shaped uncoated and coated implants in the tibia of white New Zealand rabbits. Bio-mechanical test was carried out after 2, 6 and 18 weeks healing periods. Bio-mechanical test result shows that there was increased mechanical strength (torque value) of bone-implant interface with time, and the greater increase in the torque value was noticed between 6 and 18 weeks. Also the results show that the tapered implant coated with HA<sub>p</sub> have higher removal torque values than uncoated one in different time intervals.

Tao et al., (2012) reviewed the development and recent progress for improvement of mechanical and biological properties of biomaterials (Ti, Ti alloys and biopolymers) by Plasma immersion ion implantation and deposition PIII&D method in China. The nanostructure and microstructure of surfaces have been established as a key factor affecting a number of cellular responses, such as cell

morphology, adhesion and differentiation. To ensure optimal performance of biomedical implants and to be compatible with the specific requirements of biological molecules, combination of PIII&D with other fabrication method may be required.

Pohrelyuk et al., (2013) investigated the corrosion behavior of Ti-6Al-4V alloy with nitride coatings in Ringer's solution at 36 and 40 °C. Nitride coatings of different composition, thickness and surface quality were formed because of changing nitrogen partial pressure from 1 to 10<sup>5</sup> Pa and nitriding temperature from 850 to 900 °C. The thickness and morphology of the nitride layer formed on the surface of the samples were evaluated by scanning electron microscope. Results shown that nitride coatings improve anticorrosion properties of alloy at both solution temperatures. The corrosion resistance was accompanied by measuring the open circuit potential versus time during crevice corrosion tests in Hank's solution with increase of temperature from 36 to 40 °C. Corrosion resistance of alloy increases with the content increase of TiN phase in nitride coating. Samples with nitriding showed smaller polarization resistance than untreated samples. With increase of temperature from 36 to 40 °C the corrosion resistance of alloy is determined significantly by quality of nitride coating.

### **2.3 Bone**

Bone is a mineralized connective tissue that consists of a matrix, minerals and cells. Biochemically, it is a blend of organic (35 %) and inorganic (65 %). The inorganic or mineral component consists of hydroxyapatite crystals (HA<sub>p</sub>). The hydroxyapatite gives bone its strength and rigidity (Dianne et al., 2002).



Bone tissue can be morphologically divided into two types: cortical and cancellous bone. The cortical bone structure is compact and serves mainly as mechanical support is responsible for the rigidity and strength of the skeleton. Cancellous bone is mainly responsible for the metabolic functions of bone tissue. The spaces enclosed by calcified trabeculae of spongy (cancellous) bone and the medullary cavity surrounded by compact cortical bone are filled with hematopoietic bone marrow (Muhonen et al., 2008).

### **2.3.1 Composition**

Bone is a type of highly specialized connective tissue, which is composed of cells and abundant extracellular matrix, its structural materials found in many organisms. Bone is an example of a complex natural composite materials, consisting of a mixture of organic and inorganic materials. The inorganic component consisting of (HA<sub>P</sub>) and has a composition of Ca<sub>5</sub>(PO<sub>4</sub>)<sub>3</sub>(OH), but is usually written as Ca<sub>10</sub>(PO<sub>4</sub>)<sub>6</sub>(OH)<sub>2</sub> to denote that the crystal unit cell comprises two molecules.

This inorganic component, which gives bone its solid and hard consistency, constitutes 70 % of the dry weight of bone. The organic portion of the bone consists mainly of a protein called collagen (type I) and a small amount of non-collagenous bone with its flexibility and resilience. Collagen constitutes 20 to 30 % of the weight of dry bone. Water includes 10% of remaining weight of dry bone (Sergey et al. 2011).

### **2.3.2 Macrostructure**

The structure of bone is complex, containing many constituent in both the micro and the nanorange scale. The macrostructure of bone is important because it affects the mechanical properties of the bone. Although different bones at the body

have different properties and structure, the structure of all bone at the macroscopic level may be divided into two types of hard tissue (1) cortical or compact and (2) cancellous or trabecular Figure 2.1. The cortical portion is dense (ivory like) and comprises the outer structure or cortex of the bone (Nordin et al., 2001).

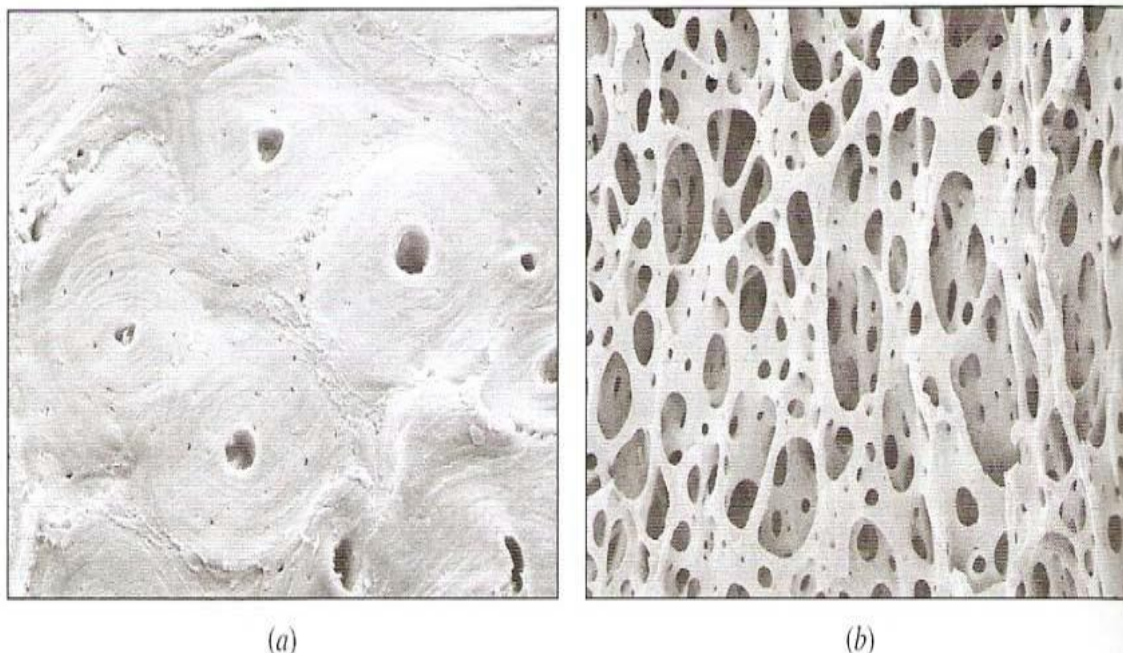


Figure 2.1: (a) The SEM image of the cortical bone from a human tibia. (Andrew Syred/Photo Researchers, Inc.) (b) A photomicrograph of cancellous bone. (Susumu Nishinaga/Photo researchers, Inc., 2001).

### 2.3.3 Mechanical Properties

Bone is a two phase composite of organic and inorganic materials. Like any other materials, its mechanical properties may be determined by performing a uniaxial tension test on it. As with other materials, an elastic range, a yield point, a plastic region and failure point will appear on the corresponding stress-strain curve. Cortical and cancellous bones have completely different mechanical properties. The cortical bone has a higher density and is stronger and stiffer than the cancellous bone; it is however more brittle. It yields and fractures when the strain exceeds 2.0 % . Cancellous (trabecular) bone however, is less dense, may sustain a strain level of 50

% before it fracture, and because of its porous structure, absorbs large amounts of energy before it fractures. Typical stress curves for cortical and trabecular bone of two different densities are given in Figure 2.2 which can clearly observe the differences in the modulus of elasticity, yield point, ductility, toughness and failure strength of various bones (Davis et al., 2003).

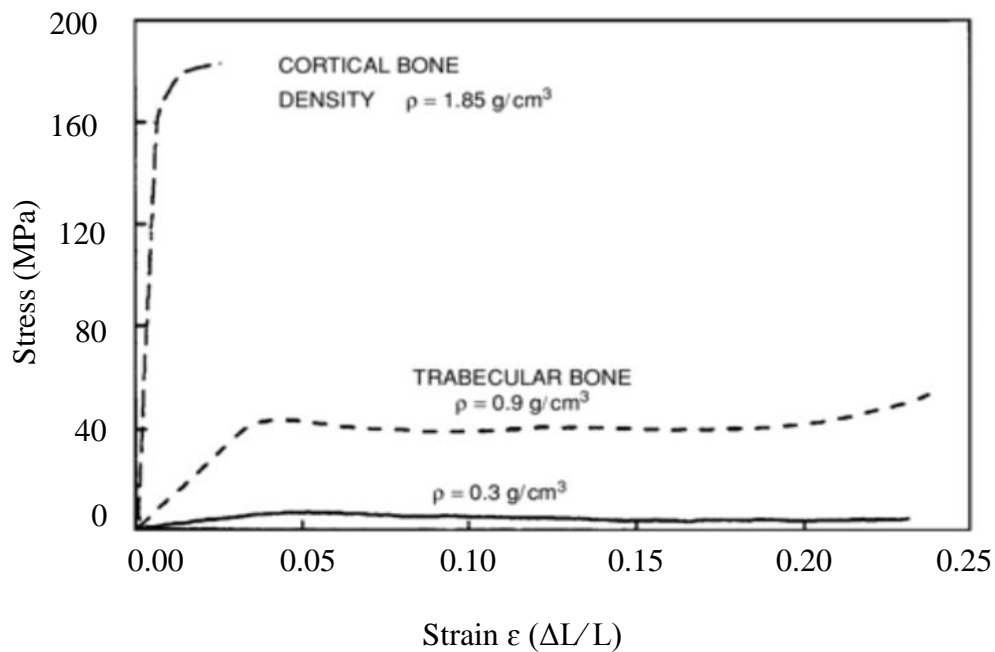


Figure 2.2: Strain curves for cortical and trabecular bones (Nordin et al., 2001).

The anisotropic behavior is observed in bone. When tensile test samples of cortical bone from the human femoral shaft were dissected in various orientations and tested uniaxially, the corresponding stress-strain curves were completely different as shown in Figure 2.3. The sample that was aligned with the longitudinal axis (L) produced the highest stiffness, strength and ductility. In contrast, the sample that was aligned transverse (T) to the longitudinal axis produced the lowest modulus of elasticity. Various bones are the strongest and the most rigid (stiff) in the direction that they are generally loaded during normal daily activities. It is worth noting that bones are generally much stronger in compressive than in tension; for instance,

cortical bone has a tensile strength of 130 MPa and a compressive strength of 190 MPa. Cancellous bones behave in a similar manner under tension and compression (Nordin et al., 2001).

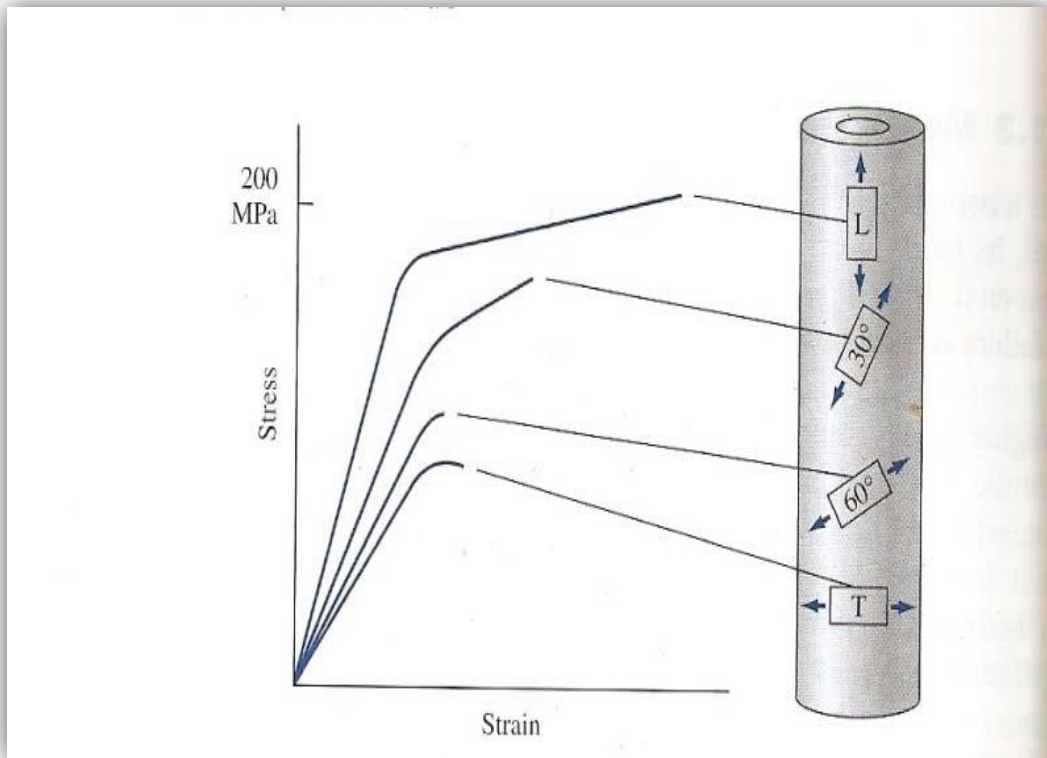


Figure 2.3: The stress strain curves for cortical bone samples of various orientations along the bone showing the anisotropic nature of bone L= longitudinal axis, T= aligned transverse (Nordin et al., 2001).

In the course of normal daily activities a human bone supports various modes of loading, including tensile, compressive, bending, torsional, shear and combined. Tensile fractures commonly occur in bones that are highly cancellous such as the bone adjacent to the achilles tendon because of the large tensile force that the calf muscle can exert on this bone. Shear fractures also occur more commonly in highly cancellous bones. Fractures under compressive loading are found mostly in the vertebrae and are more common in older patients suffering from osteoporosis

(bone porosity). Bending will cause both compressive and tensile stresses in bone (Nordin et al., 2001).

#### **2.3.4 Viscoelasticity of the bone**

Bone reacts differently under these different loading rate conditions. As the strain rate increases, a bone becomes stiffer and stronger (fails at a higher load). Over the full range of applied strain rates, cortical bone becomes stronger and its modulus of elasticity increases. At very high strain rates (impact trauma) the bone also becomes more brittle as well as stores larger amounts of energy before fracturing. This is an important issue in trauma. Under low energy fracture the energy is expended in the fracture of the bone, and the surrounding tissue does not experience significant damage. However, under high-energy fracture the excess available energy cause significant damage to the surrounding tissue.

The dependence of the mechanical behavior of the bone on strain rate is called viscoelasticity. The bone may also undergo fatigue fracture. This happens, as with other materials, when repeated cyclic loading is applied. This may be the case for an athlete undergoing weight training. After numerous loading repetitions, the muscles become tired and, as a result, the bone carries a large portion of the load. Because of the higher stresses supported by the bone, fatigue failure may occur after many cycles (Nordin et al., 2001).

#### **2.3.5 Bone Remodeling**

Bone is a complex biological material and has the ability to alter its size, shape and structure based on the mechanical demands placed upon it. The ability of bone to gain cortical or cancellous bone mass due to the elevated level of stress is

called bone remodeling and is named by Wolff's law. It is for this reason that older individuals with reduced physical activity and astronauts working in the weightless environment of space for long periods of time suffer bone loss. Moderate exercise with low weights is believed to reduce the bone – loss phenomenon in the aging population (Nordin et al., 2001).

#### **2.4 Osseointegration**

It the mode of tissue integration around a healed functioning endosteal implant in which the prime load-bearing tissue interface is bone. Osseointegration refers to the direct structural and functional connection between living bone and the surface of a load-bearing artificial implant (Dimitriou et al., 2007).

#### **2.5 Dental Implant**

Dental implants provide a unique treatment of lost dentition. This is accomplished by the insertion of relatively inert material (a biomaterial) into the soft and hard tissue of the jaws, thereby providing support and retention for dental prosthesis. Evidence of successful dental implantation can be seen in early civilizations and innovated dental practitioners who attempted the design and insertion of such devices as early as the late nineteenth and early twentieth centuries. During the developing years of implant dentists began to recognize that for implants to be successful and survive for extended periods of time in the hostile environment of stomatognathic system, there should be an effective biological adaptability between the implant material, and the tissues of the jaw (Misch et al., 1999).